Angewandte Chemie
Eine Zeitschrift der Gesellschaft Deutscher Chemiker

Supporting Information

69451 Weinheim, Germany

Direct Evidence for Hydrogen Bonding to Bound Dioxygen in a Myoglobin/Hemoglobin Model System and in Cobalt Myoglobin by Pulse-EPR Spectroscopy

Henry Dube[‡], Besnik Kasumaj[‡], Carlos Calle, Makoto Saito, Gunnar Jeschke, François Diederich*

In Memoriam Arthur Schweiger

[*] Prof. Dr. F. Diederich, Dr. M. Saito, H. Dube
Laboratorium für Organische Chemie
ETH Zürich
Hönggerberg, HCI, 8093 Zürich (Switzerland)
Fax: (+41) 44-632-1109
E-mail: diederich@org.chem.ethz.ch
Homepage: http://www.diederich.chem.ethz.ch

Dr. C. Calle, B. Kasumaj
Laboratorium für Physikalische Chemie
ETH Zürich
Hönggerberg, HCI, 8093 Zürich (Switzerland)

E-mail: besnik.kasumaj@esr.phys.chem.ethz.ch

Prof. Dr. G. Jeschke

Fachbereich Chemie

Universität Konstanz

Universitätsstrasse 10, 78457 Konstanz (Germany)

Fax: (+49) 7531-88-3139

E-mail: Gunnar.Jeschke@uni-konstanz.de

Homepage: http://dg3.chemie.uni-konstanz.de/~agje/

[‡] Both authors contributed equally to this work.

Table of Contents

Computational Details

Conformational analysis of the iron complex **1-Fe-O_2**, was conducted at the semiempirical PM5 level of theory, using the Mopac 2002 program package.[1]

The dihedral angles θ1 to θ5 indicated with blue arrows in **Figure 1SI** were adjusted to different values given in **Table 1SI.**

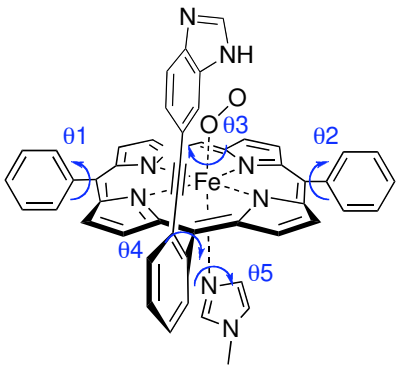

Figure 1SI: Starting geometry of **1-Fe-O_2** for conformational analysis. The dihedral angels θ1 to θ5 that were varied are indicated with blue arrows.

Table 1SI: Different dihedral angles θ1 to θ5 and their values used in the different starting geometries of **1-Fe-**O_2. All combinations of the different starting dihedral angles were used as starting points for geometry optimization.

Dihedral angle	Values in the starting geometry in °							
θ1	70	90	110					
θ2	70	90	110					
θ3	–135	–90	–45	0	45	90	135	180
θ4	70	90	110					
θ5	–135	–90	–45	0	45	90	135	180

All different combinations of the five dihedral angles led to 1728 different conformers as starting geometries for the geometry optimization of **1-Fe-**O_2. Optimization led to a considerable convergence to 93 energetically different structures. The structural overlay in **Figure 2SI** shows the calculated minimum geometry of **1-Fe-**O_2 (in orange) together with the oxygenated binding site extracted from the crystal structure of sperm whale Mb (grey, PDB code 1A6M).[2] The hydrogen atom in question was added into the crystal structure of the protein using the reported distances and angles from the neutron diffraction structure.[3] Residues appended to the porphyrin core in both the model and the protein were omitted in the picture for reasons of clarity.

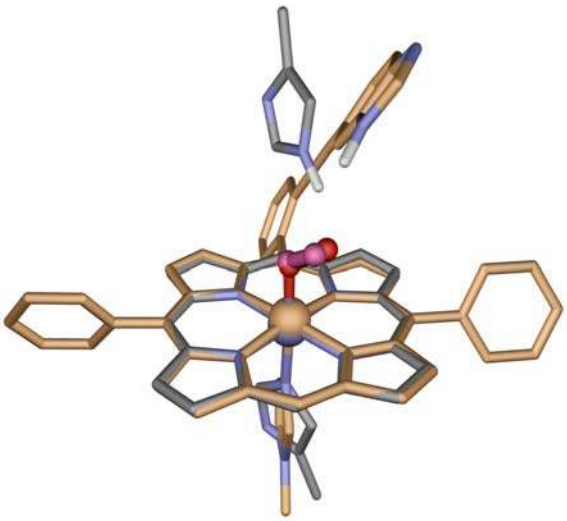

Figure 2SI: Overlay of the binding site of dioxygen-bound myoglobin extracted from the neutron diffraction structure[2,3] with the minimum energy structure of **1-Fe-**O_2.

The minimum energy structure was confirmed to be a true minimum by frequency calculations, showing six low frequencies (the "trivial modes" referring to 6 degrees of freedom for a nonlinear molecule, three for translation and three for rotation) for the structures obtained. The distances between the NH proton of the distal imidazole and each oxygen atom of dioxygen are given in **Table 2SI** together with other important geometry parameters.

Table 2SI: Comparison of the distal geometry in the calculated minimum energy structure **1-Fe**-O_2 with sperm whale Mb.[2,3]

Geometry	**1-Fe**-O_2	Mb-O_2
r(N-H···O-O) (Å)	2.41	1.98
r(N-H···O-Fe) (Å)	3.30	2.44
r(Fe-N21) (Å)	2.01	2.00
r(Fe-N22) (Å)	2.07	2.00
r(Fe-N23) (Å)	1.99	2.00
r(Fe-N24) (Å)	2.08	2.02
r(Fe-N3axial-base) (Å)	2.15	2.06
r(Fe-O) (Å)	1.71	1.81
r(O-O) (Å)	1.31	1.24
a(Fe-O-O)	120.0 °	122.5 °
d(N21-Fe-N3axial-base-C2axial-base)	−48.8 °	91.8 °
d(O-O-Fe-N21)	−79.8 °	−111.1 °

Experimental

Materials and General Methods: Reagents and solvents were purchased at reagent grade from Acros, Aldrich, and Fluka, and used as received. Tetrahydrofuran (THF) was freshly distilled from Na/benzophenone, and CH_2Cl_2 from CaH_2 under N_2, *N*,*N*-dimethylformamide (DMF) was purchased from Fluka ([H_2O] < 0.005%). All cross-coupling reactions were performed under an inert atmosphere by applying a positive pressure of N_2 or Ar. Freshly dried solvents for the glove box experiments were carefully degassed by at least 4 freeze-pump-thaw cycles ($1x10^{-3}$ mbar). Column chromatography (CC) was carried out with SiO_2 60 (particle size 0.040-0.063 mm, 230-400 mesh; Fluka) and distilled technical solvents. Thin-layer chromatography (TLC) was conducted on glass plates coated with SiO_2 60 F_{254} obtained from Merck; visualization with a UV lamp (254 or 366 nm). Melting points (m.p.) were measured on a Büchi B-540 melting-point apparatus in open capillaries and are uncorrected. "Decomp." refers to decomposition. ^{1}H NMR and ^{13}C NMR spectra were measured on a Varian Gemini 300 or on a Bruker DRX500 spectrometer at 20 °C unless otherwise stated. Chemical shifts (δ) are reported in ppm relative to the signal of tetramethylsilane (TMS). Residual solvent

signals in the ^{1}H and ^{13}C NMR spectra were used as an internal reference ($CDCl_3$: δ_H = 7.263 ppm, CD_2Cl_2: δ_H = 5.32 ppm, Me_2SO-d_6: δ_H = 2.50 ppm). Coupling constants (*J*) are given in Hz. The apparent resonance multiplicity is described as *s* (singlet), *br* (broad signal), *d* (doublet), *t* (triplet), *q* (quartet), and *m* (multiplet). Infrared spectra (IR) were recorded on a Perkin-Elmer FT1600; signal designations: vs (very strong), s (strong), m (medium), w (weak). UV/Vis spectra were recorded on a Varian Cary-5 spectrophotometer. The spectra were measured in $CHCl_3$ in a quartz cuvette (1 cm). The absorption wavelenghts (λ) are reported in nm with the extinction coefficient (ε) M^{-1} cm^{-1} in brackets; shoulders are indicated as sh. HR FT-ICR-MALDI spectra were measured on an IonSpec Ultima Fourier transform (FT) instrument with [(2*E*)-3-(4-*tert*-butylphenyl)-2-methylprop-2-enylidene]malononitrile (DCTB) or 3-hydroxypicolinic acid (3-HPA) as matrix. The most important signals are reported in *m*/*z* units with *M* as the molecular ion. Elemental analyses were performed by the Mikrolabor at the Laboratorium für Organische Chemie, ETH Zürich, with a LECO CHN/900 instrument.

Synthetic Protocols

Tetraethyl 4,4′,4′′,4′′′-[(10-{5-hydroxy-2-[(triisopropylsilyl)ethynyl]phenyl}porphyrin-5,15-diyl)bis[benzene-2,1,3-triylbis(oxy)]]tetrabutanoate (5-2H)

In a 3 L flask, equipped with a magnetic stirrer and a reflux condenser, **2** (3.32 g, 7.94 mmol), **3** (580 mg, 3.97 mmol), and **4** (4.36 g, 11.91 mmol) were dissolved in CH_2Cl_2 (2.35 L) in the dark. After addition of TFA (0.95 mL, 1.41 mmol), the mixture was stirred at 20 °C for 16 h in the dark. Chloranil (11.75 g, 47.79 mmol) was added, and the mixture was heated under reflux (40 °C) for 2 h. After cooling to 20 °C, SiO_2 (50 g) was added and the solvent was removed *in vacuo*. The residual black material was pre-purified by CC (SiO_2; CH_2Cl_2/EtOAc 95:5 → 7:3). Purification of the obtained porphyrin fraction (SiO_2; CH_2Cl_2/EtOAc 95:5) afforded **5-2H** (747 mg, 15%) as purple solid. M.p. 59 °C; ^{1}H NMR (300 MHz, $CDCl_3$): δ = 10.10 (*s*, 1H), 9.26 (*d*, *J* = 4.8 Hz, 2H), 8.93 (*d*, *J* = 4.8 Hz, 2H), 8.83-8.70 (*m*, 4H), 7.83 (*d*, *J* = 8.7 Hz, 1H), 7.72 (*t*, *J* = 8.4 Hz, 2H), 7.40 (*d*, *J* = 2.7 Hz, 1H), 7.20 (*dd*, *J* = 8.7 Hz, 2.7 Hz, 1H), 7.07 (*d*, *J* = 8.1 Hz, 2H), 7.00 (*d*, *J* = 8.1 Hz, 2H), 4.07-3.84 (*m*, 8H), 3.81-3.62 (*m*, 8H), 1.63-1.19 (*m*, 16H), 0.91-0.81 (*m*, 12H), 0.04-—0.13 (*m*, 21H), —2.83 (*br s*, 2H); ^{13}C NMR (75 MHz, $CDCl_3$): δ = 173.1, 172.8,

159.5, 159.3, 154.3, 146.8, 145.4, 132.8, 130.9, 130.6, 130.0, 123.3, 119.9, 118.8, 117.4, 115.0, 111.3, 106.9, 105.3, 105.1, 103.9, 92.6, 67.2, 60.1, 59.9, 30.3, 29.7, 24.0, 23.8, 17.7, 17.5, 13.9, 13.8, 10.3; IR (neat): 3311w, 2939m, 2863m, 2360m, 2342m, 2151w, 1728vs, 1586s, 1455vs, 1374m, 1291m, 1246s, 1178vs, 1092vs, 1029s, 970s, 957s, 931s, 882m, 833s, 803vs cm^{-1}; UV/Vis ($CHCl_3$): λ_{max} (ε) = 644 (1.700), 586 (5.700), 541 (4.500), 509 (17.900), 415 (353.500), 398 (76.600, sh), 369 (22.500); HR-MALDI-MS (3-HPA): *m/z*: 1254.5940 ($[M]^+$, $C_{73}H_{86}N_4O_{13}Si^+$, calc. 1254.5955); Anal. Calc. for $C_{73}H_{84}N_4O_{13}Si$ (1255.59): C 69.83, H 6.90, N 4.46, found: C 69.57, H 7.00, N 4.28.

{Tetraethyl 4,4′,4′′,4′′′-[(10-{5-hydroxy-2-[(triisopropylsilyl)ethynyl]phenyl}porphyrin-5,15-diyl-κ*N*^{21},κ*N*^{22},κ*N*^{23},κ*N*^{24})bis[benzene-2,1,3-triylbis(oxy)]]tetrabutanoato(2−)}zinc (5-Zn)

A 100 mL flask, equipped with a magnetic stirrer and a reflux condenser, was charged with porphyrin **5-2H** (632 mg, 0.50 mmol) and $CHCl_3$ (22 mL). $ZnOAc_2 \cdot 2H_2O$ (1.14 g, 5.19 mmol) in MeOH (22 mL) was added, and the mixture was heated under reflux (65 °C) for 1 h. After cooling, the solvent was removed *in vacuo*, CH_2Cl_2 (100 mL) was added, and the organic phase was washed with H_2O (3 x 50 mL). The combined

organic phases were dried (Na_2SO_4), concentrated *in vacuo*, and purified by CC (SiO_2; CH_2Cl_2/MeOH 98:2) to yield **5-Zn** (640 mg, 96%) as a purple solid. M.p. 65 °C (dec); ^{1}H NMR (300 MHz, $CDCl_3$): δ = 10.12 (*s*, 1 H), 9.30 (*d*, *J* = 4.4, 2 H), 8.99 (*d*, *J* = 4.4, 2 H), 8.88-8.82 (*m*, 4 H), 7.77 (*d*, *J* = 8.4, 1 H), 7.70 (*t*, *J* = 8.4, 2 H), 7.43 (*d*, *J* = 2.5, 1 H), 7.15 (*dd*, *J* = 2.5, 8.4, 1 H), 7.07 (*d*, *J* = 8.4, 2 H), 6.99 (*d*, *J* = 8.4, 2 H), 6.73 (*br s*, 1 H), 4.04-3.76 (*m*, 8 H), 3.72-3.54 (*m*, 4 H), 3.48-3.26 (*m*, 4 H), 1.54-0.83 (*m*, 16 H), 0.83 (*t*, *J* = 7.2, 6 H), 0.63 (*t*, *J* = 7.2, 6 H), —0.12-—0.25 (*m*, 21 H); ^{13}C-NMR (75 MHz, $CDCl_3$): δ = 172.8, 172.7, 159.7, 159.3, 154.1, 150.3, 150.2, 149.3, 149.1, 147.5, 132.7, 131.5, 131.2, 131.14, 131.08, 129.7, 122.8, 121.6, 119.0, 118.3, 114.8, 112.1, 107.1, 105.8, 105.7, 105.0, 92.1, 67.6, 67.5, 59.84, 59.82, 29.8, 29.6, 24.0, 23.8, 17.5, 13.9, 13.7, 10.3; IR (neat): 3421m, 2941s, 2864m, 2153w, 1734vs, 1700s, 1595s, 1560m, 1457vs, 1380m, 1301m, 1249s, 1180s, 1101vs, 1029m, 996s, 805m cm^{-1}; UV/Vis ($CHCl_3$): λ_{max} (ε) = 548 (11.800), 420 (277.000), 400 (29.300, sh), 309 (12.800); HR-MALDI-MS (3-HPA): 1316.5080 ([*M*]$^+$, $C_{73}H_{84}N_4O_{13}SiZn^+$, calc. 1316.5090); Anal. Calc. for $C_{73}H_{84}N_4O_{13}SiZn \cdot 2H_20$ (1352.53): C 64.71, H 6.55, N 4.13, found: C 64.86, H 6.65, N 3.98.

{Tetraethyl 4,4′,4′′,4′′′-([10-(5-{[6-(1*H*-imidazol-1-yl)hexyl]oxy}-2-[(triisopropylsilyl)ethynyl]phenyl)porphyrin-5,15-diyl-κN^{21},κN^{22},κN^{23},κN^{24}]bis[benzene-2,1,3-triylbis(oxy)])tetrabutanoato(2−)}zinc (6-Zn)

A 250 mL separation funnel was filled with ice-cold NaOH (85 mL, 1 M). 1-(6-Bromohexyl)-1*H*-imidazol-3-ium acetate + 2 x AcOH (700 mg, 1.70 mmol) was added, and the aqueous phase was extracted with ice cold CH_2Cl_2 (3 x 30 mL). The combined organic phases were dried (Na_2SO_4). Dry DMF (9.00 mL), **5-Zn** (640 mg, 0.49 mmol), and dry Cs_2CO_3 (636 mg, 1.95 mmol) were added and CH_2Cl_2 was removed at T ≤ 25 °C *in vacuo*. The resulting suspension was stirred at 20 °C for 14 h under N_2. Subsequently, the mixture was filtered through Celite. The Celite was washed with CH_2Cl_2 (100 mL) and the organic phase concentrated *in vacuo*. CC (2 x SiO_2; CH_2Cl_2/MeOH 99:1) afforded **6-Zn** (561 mg, 79%) as purple solid. M.p. 81–82 °C (dec); ^{1}H NMR (500 MHz, $CDCl_3$): δ = 9.95 (*s*, 1 H), 9.19 (*d*, *J* = 4.3, 2 H), 8.88 (*d*, *J* = 4.3, 2 H), 8.73 (*d*, *J* = 4.5, 2 H), 8.63 (*d*, *J* = 4.5, 2 H), 7.77 (*d*, *J* = 8.8, 1 H), 7.68 (*t*, *J* = 8.5, 2 H), 7.13 (*dd*, *J* = 1.8, 8.7, 1 H), 7.06 (*d*, *J* = 8.4, 2 H), 7.02 (*d*, *J* = 1.8, 1 H), 6.98 (*d*, *J* = 8.4, 2 H), 4.88 (*s*, 1 H), 4.02–3.92 (*m*, 4H), 3.90–3.80 (*m*, 6 H), 3.75–3.60 (*m*, 6 H), 3.58–3.49 (*m*,

2 H), 2.51 (*br t*, *J* = 5.9, 2 H), 2.22 (*br s*, 1 H), 1.92 (*s*, 1 H), 1.60 (*br s*, 2 H), 1.51–1.29 (*m*, 8H), 1.28–1.02 (*m*, 8 H), 0.94–0.85 (*m*, 2H), 0.91 (*t*, *J* = 7.2, 6 H), 0.80 (*t*, *J* = 7.2, 6 H), 0.75–0.68 (*m*, 2 H), –0.07 (*br s*, 2 H), –0.13–– 0.25 (*m*, 21 H); ^{13}C NMR (125 MHz, $CDCl_3$): δ = 173.1, 172.7, 160.2, 159.6, 155.2, 150.1, 149.9, 149.1, 149.0, 148.7, 132.2, 131.7, 131.0, 130.9, 130.5, 130.4, 129.3, 123.6, 122.8, 119.0, 118.8, 117.5, 116.6, 114.8, 110.9, 107.2, 106.2, 105.3, 104.5, 92.8, 67.6, 67.4, 66.4, 59.8, 59.7, 46.0, 29.6, 29.5, 29.3, 26.4: 24.9, 23.94, 23.89, 23.8, 17.4, 13.9, 13.8, 10.2, one signal not observed due to signal overlap; IR (neat): 3421w, 2925s, 2861m, 1730vs, 1592m, 1457s, 1379m, 1294w, 1315w, 1248s, 1183s, 1099vs, 1059m, 1029w, 993s, 800w cm^{-1}; UV/Vis ($CHCl_3$): λ_{max} (ε) = 594 (3.000), 559 (13.000), 426 (356.000), 406 (30.400, sh), 316 (14.500); HR-MALDI-MS (3-HPA): 1466.6258 ([*M*]$^+$, $C_{82}H_{98}N_6O_{13}SiZn^+$, calc. 1466.6247); Anal. Calc. for $C_{82}H_{98}N_6O_{13}SiZn$ (1469.18): C 67.04, H 6.72, N 5.72, found: C 67.15, 6.91, 5.56.

(Tetraethyl 4,4′,4′′,4′′′-{[10-(2-ethynyl-5-{[6-(1*H*-imidazol-1-yl)hexyl]oxy}phenyl)porphyrin-5,15-diyl-κ*N*^{21},κ*N*^{22},κ*N*^{23},κ*N*^{24}]bis[benzene-2,1,3-triylbis(oxy)]}tetrabutanoato(2–))zinc (7-Zn)

A 10 mL flask, equipped with a magnetic stirrer and a septum, was charged with **6-Zn** (120 mg, 0.08 mmol) and THF (3.00 mL). *n*Bu_4NF (0.40 mL, 1 M in THF, 0.40 mmol) was added dropwise. After stirring for 40 min at 20 °C, the conversion was complete. The mixture was poured into a mixture of EtOAc/saturated aqueous NH_4Cl solution (150 mL, 2:1), and the phases were separated. The aqueous phase was extracted with EtOAc (3 x 50 mL). The combined organic phases were dried (Na_2SO_4) and concentrated *in vacuo*. Purification by CC (SiO_2; CH_2Cl_2/MeOH 98:2) afforded **7-Zn** (100 mg, 93%) as purple solid. M.p. 88-90 °C (dec); ^{1}H NMR (500 MHz, $CDCl_3$): δ = 9.96 (*s*, 1 H), 9.19 (*d*, *J* = 4.4, 2 H), 8.89 (*d*, *J* = 4.4, 2 H), 8.78 (*d*, *J* = 4.5, 2 H), 8.65 (*d*, *J* = 4.5, 2 H), 7.79 (*d*, *J* = 8.9, 1 H), 7.68 (*t*, *J* = 8.5, 2 H), 7.15 (*dd*, *J* = 1.8, 7.7, 1 H), 7.07 (*d*, *J* = 1.8, 1 H), 7.04 (*d*, *J* = 8.5, 2 H), 7.00 (*d*, *J* = 8.5, 2 H), 4.92 (*s*, 1 H), 4.05-3.92 (*m*, 4 H), 3.91-3.82 (*m*, 6 H), 3.72-3.56 (*m*, 6 H), 3.55-3.47 (*m*, 2 H), 2.52 (*br t*, *J* = 5.7, 2 H), 2.31 (*s*, 1H), 2.24 (*s*, 1 H), 2.00 (*s*, 1 H), 1.60 (*br s*, 2 H), 1.48-1.02 (*m*, 16 H), 0.91 (*t*, *J* = 7.1, 6 H), 0.94-0.87 (*m*, 2H), 0.79 (*t*, *J* = 7.1, 6 H), 0.76-0.69 (*m*, 2 H), –0.05 (*br s*, 2 H); ^{13}C NMR (125 MHz, $CDCl_3$): δ = 173.1, 172.7, 160.0, 159.6, 155.4, 150.3, 149.9, 149.3, 148.8, 148.5, 132.6, 131.7, 131.0, 130.8, 130.6, 130.5, 129.4, 123.6, 122.4,

118.7, 117.7, 116.8, 115.0, 111.02, 110.98, 105.9, 105.2, 104.8, 83.5, 79.6, 67.5, 67.4, 66.3, 59.8, 59.7, 46.1, 29.7, 29.5, 29.3, 26.3, 24.8, 24.0, 23.9, 23.8, 13.9, 13.8; IR (neat): 3290w, 3117w, 2932m, 2870w, 1732vs, 1593m, 1520m, 1456vs, 1382m, 1297m, 1247s, 1182vs, 1099vs, 1057m, 1030m, 992vs, 940w, 910w, 840w cm^{-1}; UV/Vis ($CHCl_3$): λ_{max} (ε) = 597 (4.300), 560 (18.500), 427 (502.000), 406 (41.600, sh), 314 (22.900); HR-MALDI-MS (3-HPA): 1310.4918 ($[M]^+$, $C_{73}H_{78}N_6O_{13}Zn^+$, calc. 1310.4913); Anal. Calc. for $C_{73}H_{78}N_6O_{13}Zn$ (1312.84): C 66.79, H 5.99, N 6.40, found: C 66.69, H 6.17, N 6.24.

(Tetraethyl 4,4′,4′′,4′′′-{[10-(2-(1*H*-benzimidazol-6-ylethynyl)-5-{[6-(1*H*-imidazol-1-yl)hexyl]oxy}phenyl)porphyrin-5,15-diyl-κN^{21},κN^{22},κN^{23},κN^{24}]bis[benzene-2,1,3-triylbis(oxy)]}tetrabutanoato(2−))zinc (1-Zn)

A dry, N_2-flushed 10-mL Schlenk tube, equipped with a magnetic stirrer and a septum, was charged with **7-Zn** (80 mg, 0.06 mmol), 5(6)-iodobenzimidazole (58 mg, 0.24 mmol), CuI (16 mg, 0.08 mmol), and $[Pd(PPh_3)_4]$ (58 mg, 0.05 mmol). The Schlenk tube was carefully evacuated again and purged with N_2 twice. DMF (3.00 mL) and NEt_3 (5.00 mL) were added, and the mixture was stirred 4 h at 100 °C under N_2. A

saturated aqueous solution of NH_4Cl (50 mL) and EtOAc (50 mL) were added and the phases separated. The aqueous phase was extracted with EtOAc (2 x 50 mL), and the combined organic phases were dried (Na_2SO_4) and concentrated *in vacuo*. Purification by CC (SiO_2 CH_2Cl_2/MeOH 97:3), preparative GPC (SX-1, THF) followed again by CC (2 x SiO_2; CH_2Cl_2/MeOH 100:0.5 → 100:1 → 100:2) afforded **1-Zn** (55 mg, 51%) as purple solid. M.p. 96-97 °C (dec); ^{1}H NMR (300 MHz, $CDCl_3$): δ = 9.84 (*s*, 1 H), 9.06 (*br s*, 2 H), 8.71 (*br s*, 2 H), 8.59 (*br s*, 4 H), 7.72-7.48 (*m*, 4 H), 7.19-7.07 (*br s*, 1 H), 7.01-6.74 (*m*, 5 H), 6.5 (*br s*, 2 H), 5.3 (*br s*, 1 H), 4.06-3.32 (*m*, 19 H), 2.74 (*br*, 2 H), 2.59 (*br*, 1 H), 2.09 (*br*, 1 H), 1.65 (*br*, 2 H), 1.54-0.52 (*m*, 34 H); ^{13}C NMR (75 MHz, $CDCl_3$): δ = 173.0, 172.6, 159.6, 158.9, 156.7, 149.9, 149.7, 148.9, 148.6, 148.0, 136.5, 135.8, 133.3, 130.9, 130.8, 130.7, 130.6, 129.4, 127.4, 122.1, 120.0, 119.8, 118.4, 117.2, 116.0, 114.1, 113.4, 111.2, 105.8, 105.7, 104.8, 91.2, 89.3, 67.7, 67.3, 67.0, 60.3, 59.6, 46.9, 30.5, 29.4, 29.3, 28.4, 26.0, 25.4, 23.8, 23.3, 14.3, 13.8, four signals not observed due to signal overlap; IR (neat): 3322w, 3111m, 2975m, 2939m, 2869m, 1733vs, 1594s, 1456vs, 1381m, 1321m, 1293m, 1249s, 1187s, 1097vs, 1058m, 1030m, 992s, 940w, 907w, 840w, 830w, 792m cm^{-1}; UV/Vis ($CHCl_3$): λ_{max} (ε) = 599 (3.900), 560 (18.200),

427 (477.000), 406 (39.900, sh), 320 (46.600); HR-MALDI-MS (DCTB): 1427.5371 ([*M*H]$^+$, $C_{80}H_{83}N_8O_{13}Zn^+$, calc. 1427.5366); Anal. Calc. for $C_{80}H_{82}N_8O_{13}Zn$ (1428.94): C 67.24, H 5.78, N 7.84, found: C 67.50, H 6.03, N 7.58.

Deuterium Exchange of the Zinc Complexes

Deuterium exchange was tested by stirring a solution of **1-Zn** in CD_2Cl_2 with D_2O for 10 s. Only one single proton peak at 5.80 ppm (**Figure 3SI and Figure 4SI**) disappeared in the ^1H NMR spectra and appeared again after stirring the same solutions with H_2O.

(Tetraethyl 4,4′,4′′,4′′′-{[10-(2-(1*H*-benzimidazol-6-ylethynyl)-5-{[6-(1*H*-imidazol-1-yl)hexyl]oxy}phenyl)porphyrin-5,15-diyl-κ*N*^{21},κ*N*^{22},κ*N*^{23},κ*N*^{24}]bis[benzene-2,1,3-triylbis(oxy)]}tetrabutanoato(2−))cobalt (1-Co)

All processes were carried out under N_2 atmosphere in the dark. To a solution of **1-Zn** (21 mg, 15.00 μmol) in degassed $CHCl_3$ (4.80 mL), TFA (0.24 mL, 368 mg, 3.2 mmol) was added. The mixture was stirred for 12 min. To the green solution, degassed saturated aqueous solution of $NaHCO_3$ (4.80 mL) was added and the two-phase mixture was stirred vigorously until the organic phase turned brown. The colorless aqueous phase was removed by means of a syringe with a

long, thin needle. The organic phase was washed with degassed H_2O (2 x 4.80 mL) in a similar manner and directly subjected to column chromatography (Al_2O_3 neutral; CH_2Cl_2 → CH_2Cl_2/MeOH 20:1), the product containing fractions were filtered through cotton, and the solvent was removed *in vacuo*. The free base **1-2H** (20 mg, quant.) was obtained as brown amorphous solid.

The following steps were carried out in a glove box (oxygen level < 2 ppm, water level < 5 ppm) with carefully degassed and dried solvents. To a degassed solution of **1-2H** (20 mg, 15.00 μmol) in degassed THF (3.30 mL), $CoCl_2$ (18 mg, 140 μmol) and degassed 2,6-lutidine (3 drops) were added and the mixture was stirred in the dark for 12 h. Samples (0.60 mL) of the mixture were directly subjected to CC (degassed Al_2O_3 neutral, CH_2Cl_2 → CH_2Cl_2/MeOH 20:1) to give a mixture of predominantly **1-Co^{II}** and some **1-Co^{III}**, which was analyzed by UV/Vis-spectroscopy. M.p. 152 °C (dec); IR (neat): 2924m, 2848w, 1726 s, 1664w, 1594m, 1494w, 1456s, 1370m, 1288m, 1248s, 1179s, 1095vs, 1063s, 1025m, 1003s, 817w; UV/Vis ($CHCl_3$): **1-Co^{II}**, λ_{max} = 408, 529; **1-Co^{III}**, λ_{max} = 429, 540; HR-MALDI-MS (HPA): 1421.5310 ([*M*]$^+$, $C_{80}H_{82}CoN_8O_{13}^+$, calc. 1421.5328.

The solvent was removed *in vacuo*, and fresh CH_2Cl_2 (0.10 mL) was added. The resulting solution of **1-Co** was directly used for the EPR.

Reduction Protocol

Complex **1-Co** was found to be predominantly in the Co^{II} oxidation state after CC. However, an additional reduction step was introduced in order to achieve comparable conditions (wet solvent) with the sample obtained after deuterium exchange.

After removing the solvent from the CC purification, the residual solid was dissolved in degassed CH_2Cl_2 (1.00 mL) and stirred vigorously with an aqueous solution of $Na_2S_2O_4$ (20 mg in 1.00 mL H_2O) for 30 min. The organic phase was analyzed by UV/Vis-spectroscopy showing no alteration of the spectrum with Co^{II} still being predominant in the solution (**Figure 5SI** and **Figure 6SI**). The solvent was again removed *in vacuo*, and fresh CH_2Cl_2 (0.10 mL) was added.

The additional reduction step could be omitted for **1-Co**, in order to obtain an H_2O-free sample. Therefore, dry CH_2Cl_2 and MeOH were used for the CC. Residual solvent from the CC was removed *in vacuo* and the resulting **1-Co** was dried at ultra high vacuum ($4x10^{-6}$ mbar) for 24 h before

adding fresh, dry CH_2Cl_2 (0.10 mL) to prepare the EPR samples. Complex **1-Co** was also measured in CD_2Cl_2 as solvent.

Deuterium Exchange of the Cobalt Complex

Deuterium exchange was achieved by vigorously stirring a solution of **1-Co** (4 mg) in CH_2Cl_2 (1.00 mL) with $Na_2S_2O_4$ (20 mg) in D_2O (1.00 mL) for 30 min. The organic phase was directly used for the measurements.

Preparation of the Dioxygen Adducts

After recording the Co^{II} CW EPR spectrum, a 0.10 mL sample of **1-Co** in CH_2Cl_2 was warmed up to 20 °C and pure O_2 was bubbled through the solution by means of an O_2-filled balloon and a long needle for 25 s, after which no residual Co^{II} signal was visible in the X-band CW EPR spectrum. Immediately after oxygenation, the solution was frozen in liquid N_2 and put into the spectrometer at 120 K.

No CW EPR spectra of the H_2O-free sample of **1-Co** were recorded in order to avoid H_2O condensing in the sample tube during warm-up after CW EPR measuring. Instead, a sample of **1-Co** was subjected to O_2 for 25 s at 20 °C, directly after preparation, immediately frozen in liquid N_2, and Davies-ENDOR spectra were recorded.

Spectra

^{1}H NMR Spectra of the Deuterium Exchange of 1-Zn

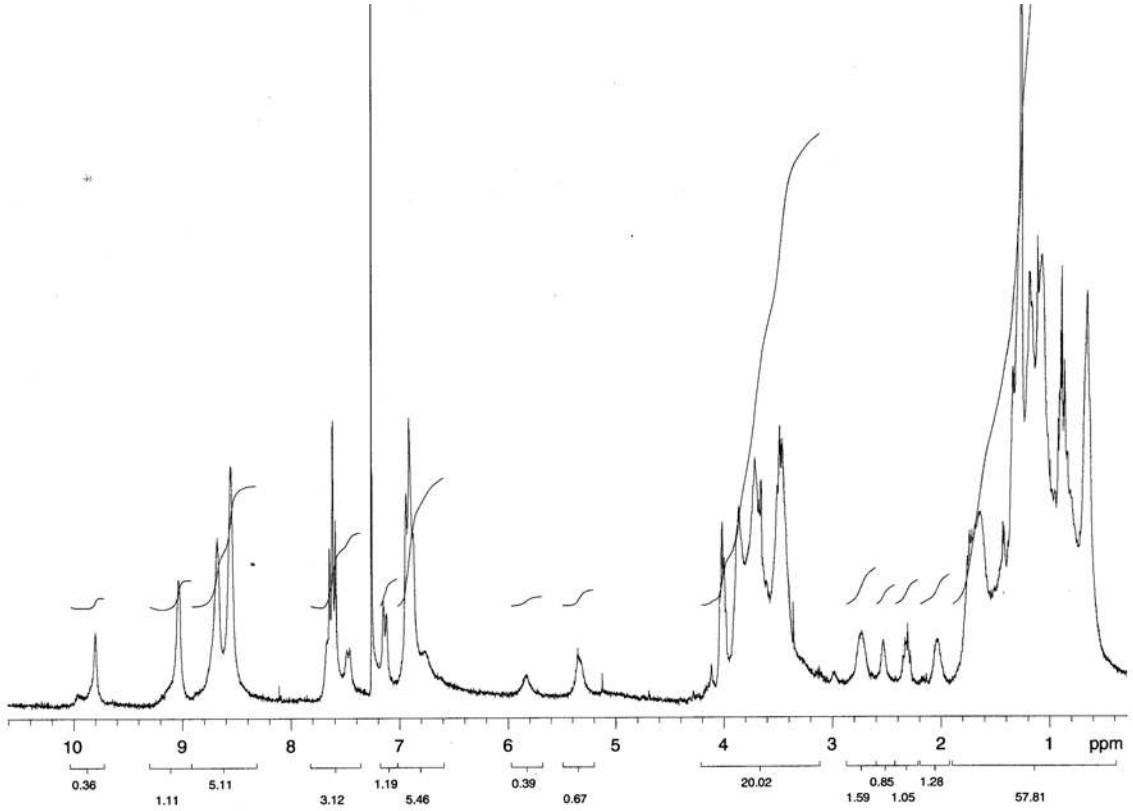

Figure 3SI: ^{1}H NMR spectrum (300 MHz, $CDCl_3$, 20 °C) of **1-Zn.** The broadness of the spectrum is caused by a dynamic equilibrium between intramolecular ligation of the zinc(II) ion by the alkyl-tethered imidazole and intermolecular ligation by the distal benzimidazole. However, the intramolecular ligation by the alkyl-tethered imidazole is considerably favored over the intermolecular ligation, which is clearly visible by the indicative shifts of the imidazole protons at 2.09 ppm, 2.59 ppm, and 5.30 ppm, as well as the indicative shift of the alkyl-chain of the

tether at 2.74 ppm.[4] Heating to 35 °C and cooling down to –20 °C did not change the ^{1}H NMR spectrum of **1-Zn**.

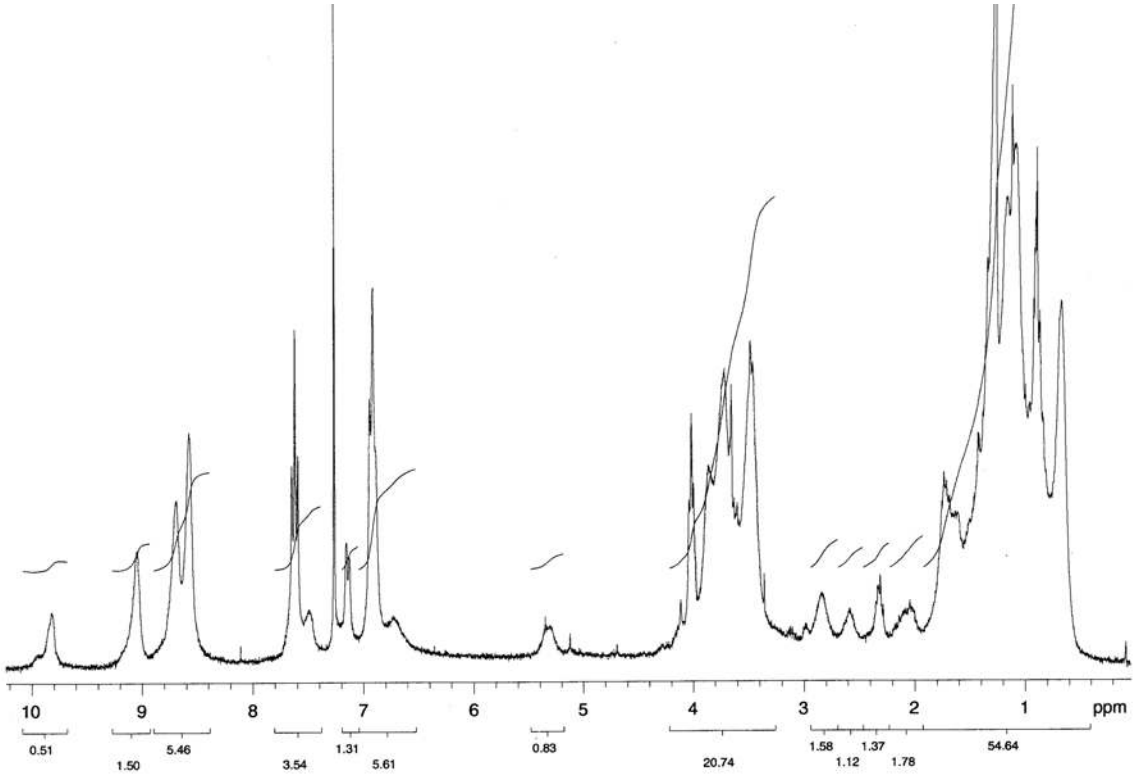

Figure 4SI: ^{1}H NMR spectrum (300 MHz, $CDCl_3$, 20 °C) of **1-Zn** after 10 s shaking with D_2O. Only the peak at 5.80 ppm has disappeared.

UV/Vis Spectra of 1-Co

1-Co was found predominantly in the Co^{II} oxidation state directly after the insertion reaction.

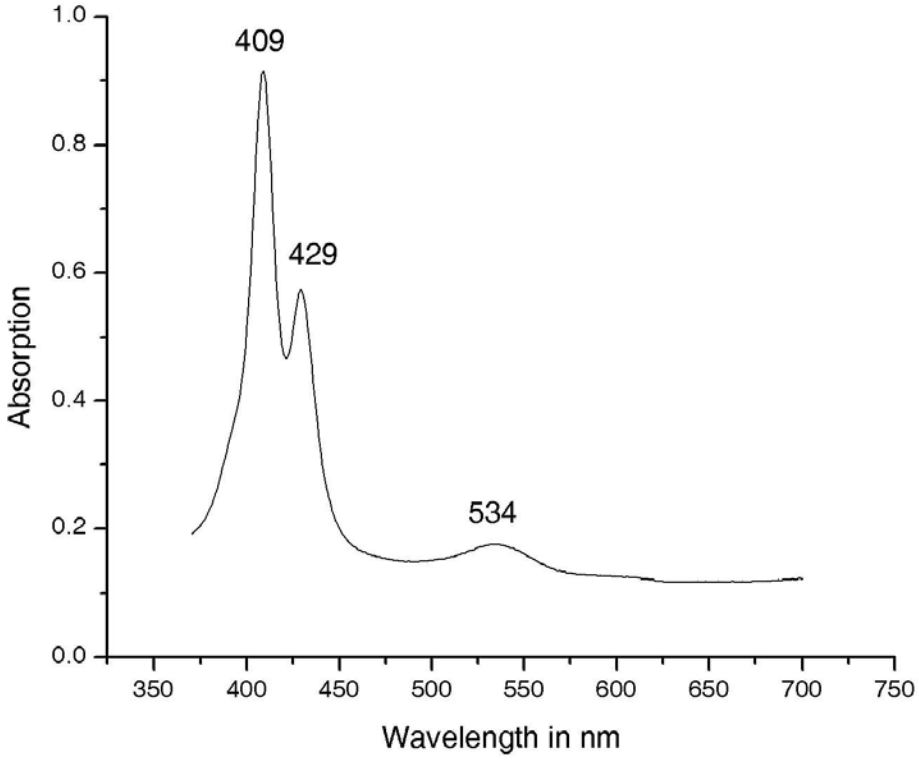

Figure 5SI: UV/Vis spectrum (CH_2Cl_2, 20 °C) of **1-Co** after cobalt insertion. Co^{II} is the predominant oxidation state.

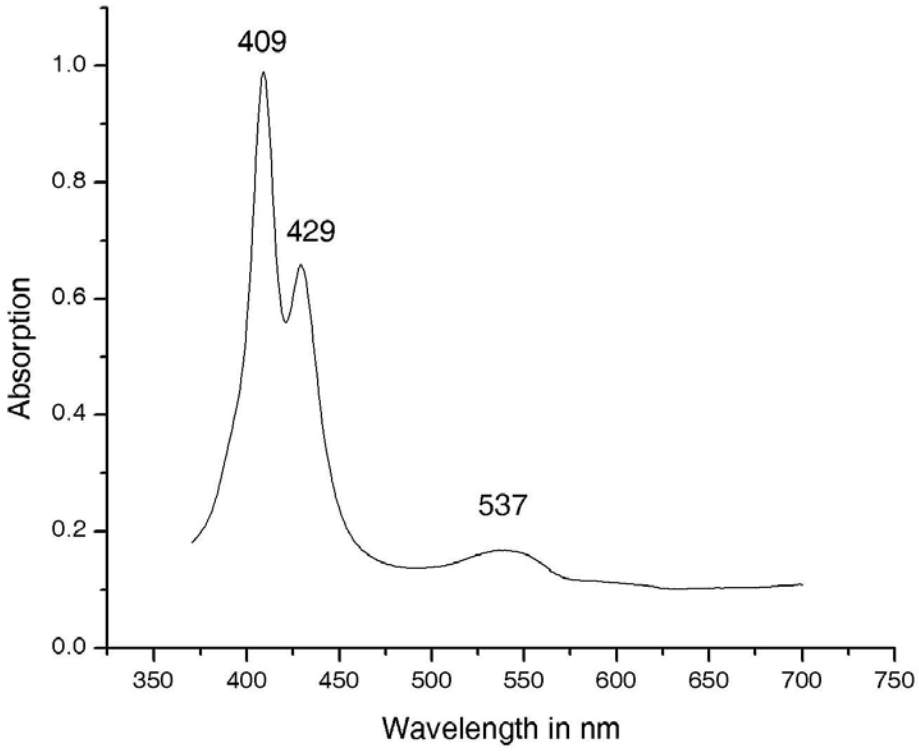

Figure 6SI: UV/Vis spectrum (CH_2Cl_2, 20 °C) of **1-Co** after dithionite reduction. There are still remaining Co^{III} species in the solution.

EPR Studies

General

Continuous wave (CW) EPR spectra were recorded on a Bruker ELEXYS E500 spectrometer at X-band microwave frequency (approximately 9.8 GHz) in frozen solution at 120 K.

For the model complex **1-Co**-O_2 and Co-Mb-O_2 2- and 3-pulse ESEEM, 4-pulse-, matched- and SMART-HYSCORE, hyperfine-decoupled ESEEM, Mims and Davies-ENDOR were tried to measure the proton hyperfine couplings at X-band frequencies. None of these established pulse-EPR methods allowed for a complete detection of the proton hyperfine splittings. The reason is a severe cross suppression effect, which is present in both **1-Co**-O_2 and Co-Mb-O_2 because of the presence of several strong suppressors.[5] However, we were able to measure parts of the largest and exchangeable proton hyperfine splitting by X-band 6-pulse HYSCORE, which suffers less strongly from cross suppression than the standard 4-pulse HYSCORE.[6] For the 6-pulse HYSCORE experiment we used nominal pulse lengths of 12 ns and 24 ns ($\pi/2$ and π) and $\tau_1 = \tau_2 = 112$ ns, an eight step phase cycle was used.

In order to avoid the strong modulation depths (and therefore the severe cross suppression) at X-band frequencies, the proton hyperfine splittings were measured at Q-band frequency where the modulation depths (and also the cross suppression effect) is weaker.

Davies-ENDOR spectra were recorded on a home-built spectrometer at Q-band microwave frequency (approximately 34.7 GHz) in frozen solution at 10 K (**1-Co**-O_2) or 13 K (Co-Mb-O_2). Field-swept FID-integral-detected EPR spectra were recorded using a weak 500 ns preparation pulse and a 40 ns $\pi/2$ pulse for the detection. For Davies-ENDOR, the applied preparation pulse length were 160 ns and 80 ns, followed by an rf π-pulse of 8.5 μs (sandwiched by waiting times of 500 ns and 1000 ns respectively), and the read-out sequence 40 ns ($\pi/2$ pulse) - 200 ns free evolution time - 80 ns (π-pulse). The orientations contributing to the spectra are each shown next to the spectra projected on unit spheres. The observer positions are indicated on the EPR spectra insets in the respective figures. Deviations of signal-to-noise ratios in different spectra were - amongst other reasons - caused by a phase drift during the data acquisition and hampered quantitative analysis of difference spectra.

EPR Spectra of 1-Co-O_2

X-Band CW Spectra

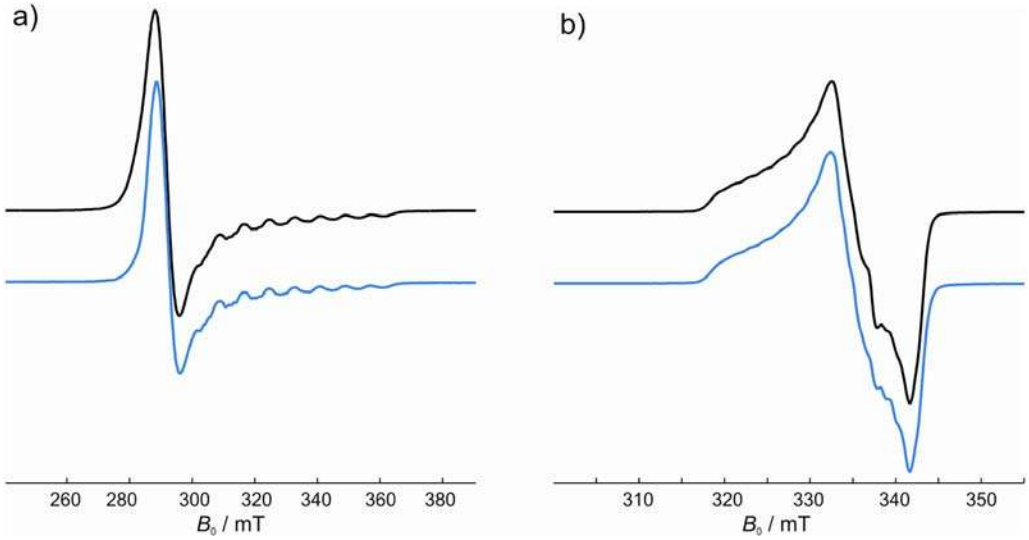

Figure 7SI: X-band frozen-solution CW EPR spectra of **1-Co** in CH_2Cl_2 (black), after D_2O exchange in CH_2Cl_2 (blue). a) Co^{II} species. b) **1-Co**-O_2 complexes.

Q-Band Davies-ENDOR Spectra

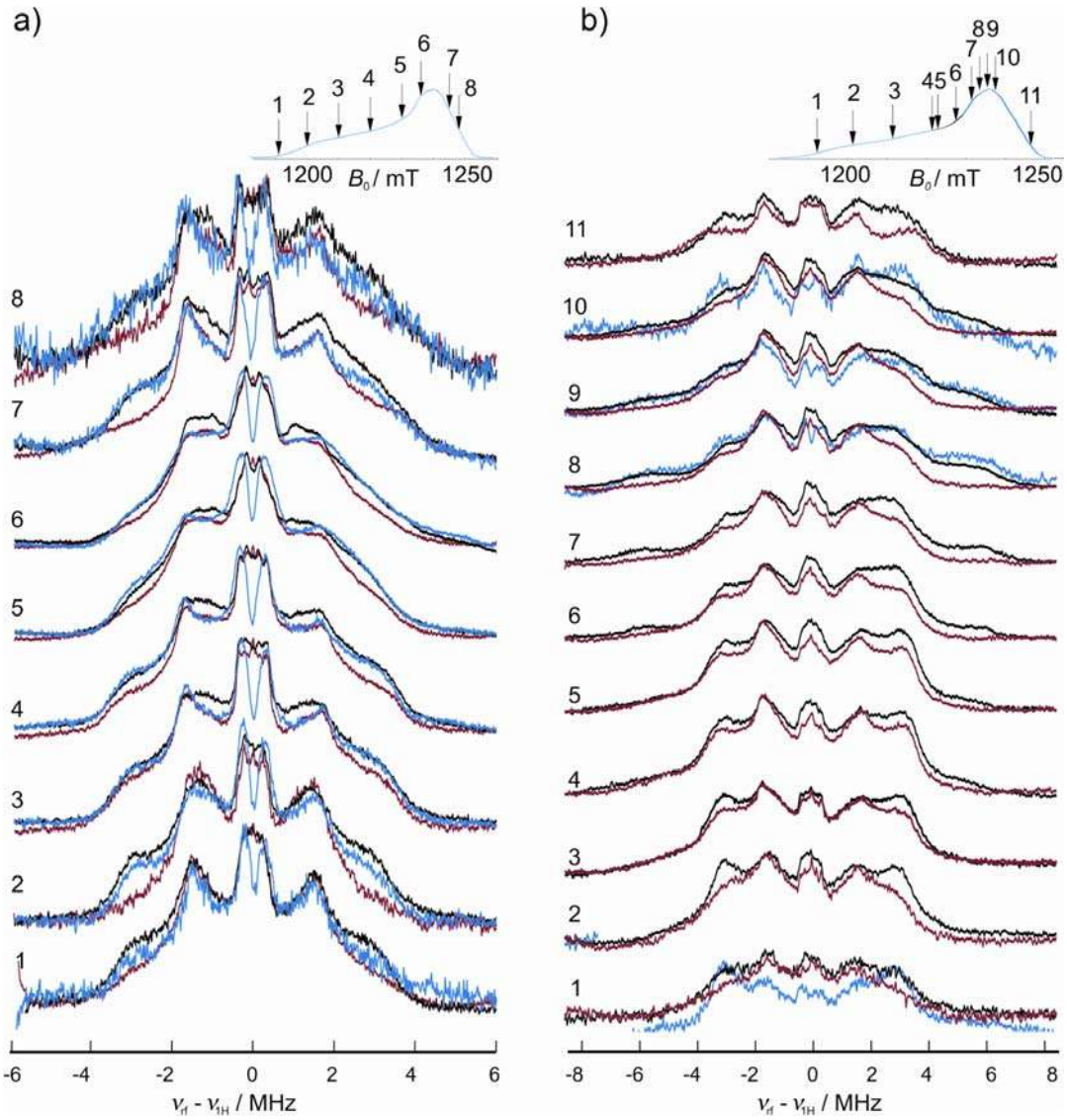

Figure 8SI: Frozen-solution Davies-ENDOR spectra of **1-Co**-O_2 in CH_2Cl_2 (black), in CD_2Cl_2 (blue) and after D_2O exchange in CH_2Cl_2 (red). Observer positions are indicated on the FID-integral-detected EPR spectra in the insets. a) Preparation pulse length = 160 ns. b) Preparation pulse length = 80 ns.

X-Band 6-Pulse HYSCORE of 1-Co-O_2

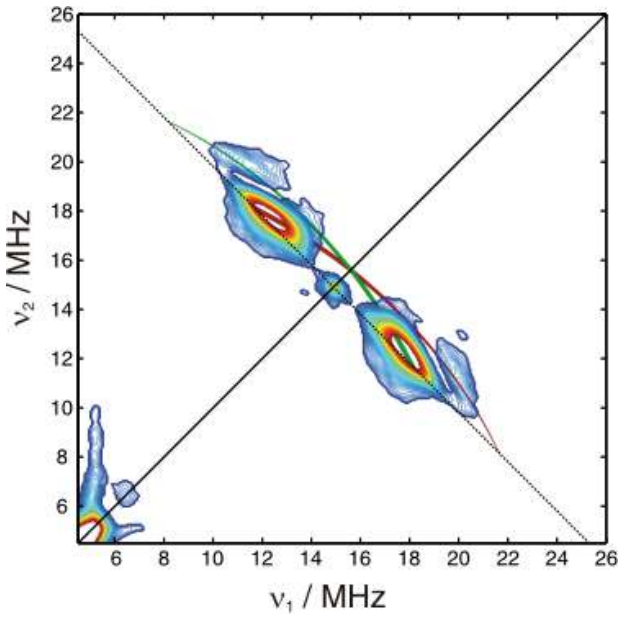

Figure 9SI: X-band frozen-solution 6-Pulse HYSCORE spectrum of **1-Co-**O_2 in CH_2Cl_2 at 20 K at g = 2.0245. The off anti-diagonal ridges stemming from the largest and exchangeable proton hyperfine splitting can clearly be distinguished from the residual anti-diagonal proton splittings. The simulated ridges (green and brown line) show the real signal extension. Simulation parameters were taken from **Table 3SI.**

Simulations of EPR Spectra of 1-Co-O_2

General

The principal values of the g matrix, [g_x, g_y, g_z]= [2.0027 ± 0.0005, 1.989 ± 0.001, 2.0723 ± 0.0005], the principal values of the metal hyperfine tensor A^{Co} = [—54, —28, —28] MHz ± 2 MHz and its relative orientation to the g-frame, determined by the Euler angles (α, β, γ) = (0° ± 10°, 70° ± 10°, 0° ± 20°), are close to values found for the dioxygen adducts of Co^{II} corrin and tetraphenylporphyrin complexes.[7b,c]

For the CW EPR simulation[7a] (**Figure 10SI**) the simulated spin system contained one electron (S = 1/2) and a ^{59}Co nucleus (I = 7/2). The axially and equatorially coordinating nitrogen nuclei were not taken into account as the small hyperfine couplings are only contributing to the overall line width, but the splittings are not resolved.

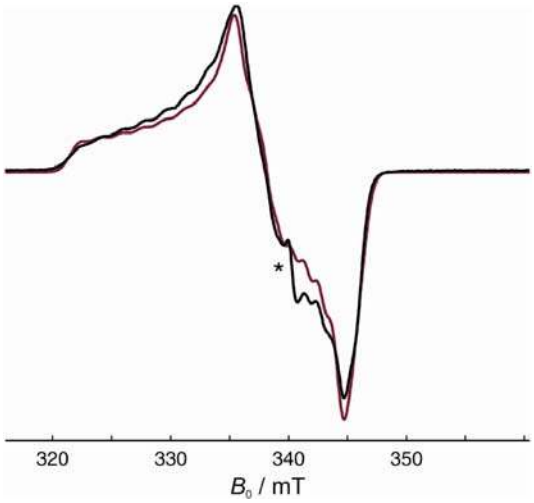

Figure 10SI: Simulation (red) of the frozen-solution CW EPR spectrum of **1-Co**-O_2 (black). * Radical contamination.

ENDOR Spectra Simulations

ENDOR simulations[7a] were performed assuming a single unpaired electron and proton nuclei (I = 1/2). No difference could be observed between simulated spectra obtained for this spin system and the one additionally containing a ^{59}Co nucleus (I = 7/2, A^{Co} = [−58 −28 −28]). A Gaussian excitation line width of 100 MHz was used in the simulations, assuming that the resonator band width limits the excitation of contributing spin packets. The ENDOR line widths were modeled using a Gaussian distribution of the widths of Lorentzian lines. The ideal Lorentzian line width is 0.12 MHz ($1/t_{\pi,rf}$). The closer a proton is located to a (virtual) spin density centre, the more pronounced the effect of conformational differences on its hyperfine splitting is. Thus, different conformers in frozen solution were accounted for with different Gaussian weighting functions of the Lorentzian lines semi-quantitatively adapted to the splitting magnitude.[8a,d-g]

Simulations of the ENDOR spectra were performed, with the main focus on the largest experimentally observable hyperfine splitting stemming from the exchangeable proton. However, also an assignment of some of the other protons could be achieved as their spectral features were sufficiently well resolved. The assignments and obtained parameters shown in **Figure 11SI** and **Table 3SI** were found by comparing simulated and experimental spectra by visual inspection. In order to separate some of the overlapping proton peaks and thus facilitate the assignment, difference spectra were computed. For the separation of the exchangeable proton peaks difference spectra of **1-Co**-O_2 before and after D_2O exchange in the solvent CH_2Cl_2 were chosen (**Figure 12SI**). For the separation of the solvent peaks, difference spectra of **1-Co**-O_2 in CH_2Cl_2 and in CD_2Cl_2 were chosen (**Figure 13SI**). Thus, besides the largest and exchangeable proton hyperfine splitting (proton 1) also the solvent peaks (proton 2, 3 and 4, see **Figure 11SI**) could be well resolved and the matrix peak observed. The difference spectra of **1-Co**-O_2 before and after D_2O exchange in CH_2Cl_2 contain a matrix part, which is presumably caused by distant H_2O in the solvent, stemming from the reduction step (see reduction protocol). The hyperfine splitting of proton 5 was clearly visible in the ENDOR spectrum of **1-Co**-

O_2 measured in CD_2Cl_2 and could be caused by β-protons of the porphyrin macrocycle or protons at comparable distances.[9] Values for proton 6 were taken from the literature, where similar results were found stemming from the *ortho*-protons of the proximal pyridine in the dioxygen adduct of a β-octaethylporphyrinato-Co^{II} (CoOEP) complex.[9] Proton splittings of comparable magnitude as of the protons 7 to 10 are reported in literature for solvent interactions if dioxygen adducts of Co^{II} porphyrins are used, which do not posses distal residues, e.g. CoOEP.[9] However, the comparison of the difference spectra of **1-Co**-O_2 in CH_2Cl_2 and CD_2Cl_2 revealed that the splittings 7 to 10 MHz (±3 - ±8 MHz) are not caused by interactions with the solvent. Thus, it can be concluded that these protons belong either to the ester side arms or to the non-exchangeable protons of the distal residue. The assignment of the second largest splitting 7 to a non-exchangeable proton of the distal residue was made by the reasoning that if there is a distal hydrogen bond in complex **1-Co**-O_2, one aromatic non-exchangeable proton of the distal benzimidazole is simultaneously forced to be rather close to bound dioxygen (**Figure 11SI**). The three additional proton hyperfine splittings 8 to 10 were sufficiently well resolved to obtain qualitatively satisfying “fits” of the experimental

spectra. Given the constitution of **1-Co**-O_2 with the distal benzimidazole and the flexible distal ester side arms, three different distal protons close to bound dioxygen are possible (**Figure 11SI**). With the available data assignments of the proton splittings 8 to 10 were not possible. Potentially, more sophisticated EPR experiments in combination with site-selective deuterium exchange might allow for a more accurate assignment.[10]

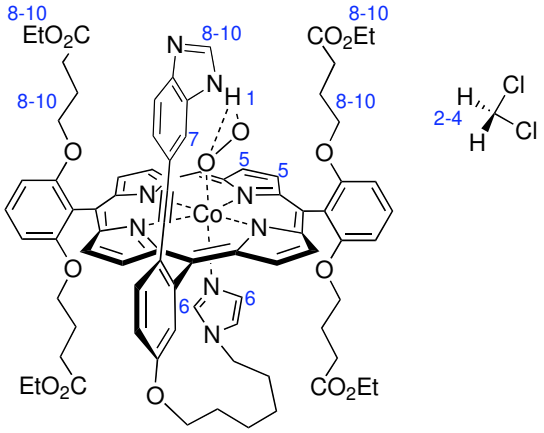

Figure 11SI: Assignments of the intra-molecular proton hyperfine splittings of **1-Co-**O_2**.** Proton 7 is forced close to bound dioxygen upon formation of the distal hydrogen bond.

Table 3SI: Principal values of proton hyperfine interactions A^{H} in complex **1-Co-**O_2 in MHz and qualitative assignments of these protons. The Euler angles α, β, and γ describe the orientation with respect to the *g*-frame, and have an error of ± 10° - 20°. Additionally, the Gaussian line width (Δw_{Gauss}) and the distances *d* to the virtual spin density center are given. The distances *d* are determined from the dipolar part of the hyperfine interaction. * The quality of the spectra did not allow for a detailed assignment of these protons.

Proton/Position		A_x /MHz	A_y /MHz	A_z /MHz	Err.	α/°	β/°	γ/°	Err.	d/Å	Δw_{Gauss}
1	NH proton	−6.8	−6.0	13.5	± 0.5	0	105	0	10	2.3	1
2	Solvent	2.4	1.3	1.3	± 0.2	0	0	0	10	6.0	0.6
3	Solvent	3.2	2.0	2.0	± 0.2	0	20	0	10	5.8	0.6
4	Solvent	6.0	2.5	2.5	± 0.2	40	30	−10	20	4.1	0.8
5	β-Position or phenyl	0.75	−0.55	−0.55	± 0.05	0	90	0	10	5.8	0.4
6	Proximal base[9]	1.17	−1.07	−1.02	± 0.01	0	90	0	20	4.8	0.6
7*	Distal residue	−3.6	−3.6	7.2	± 0.2	0	40	0	20	2.8	1
8*	Ester/distal residue	3.0	6.0	3.0	-	20	30	0	20	4.0	1
9*	Ester/distal residue	3.0	3.0	6.5	-	0	30	0	20	4.1	1
10*	Ester/distal residue	3.6	2.6	2.6	-	10	0	0	20	6.2	0.8

Simulations of the Davies-ENDOR spectra (**Figure 12SI** to **Figure 15SI**) were performed using identical parameters in all simulations as it is described in the following: In a first step, each proton hyperfine interaction was simulated individually for all the different field positions (see details in **Table 3SI**). The Gaussian line widths were assigned to 1.0 MHz for protons 1 (Solution 1 and Solution 2) and protons 7 to 9, 0.6 MHz for protons 2, 3 and 6, 0.8 MHz for protons 4 and 10 and 0.4 MHz for proton 5. After that, the intensity of each spectrum was multiplied with the hyperfine contrast selectivity function[8c]

$$w(\nu_{rf}) = \frac{2\sqrt{2}t_{\pi}\,|\nu_{rf} - \nu_{1\mathrm{H}}|}{1/2 + (2t_{\pi}\,|\nu_{rf} - \nu_{1\mathrm{H}}|)^2} + 0.05\ ,$$

where a constant threshold of 5 % was added in order to account for imperfections (see **Figure 14SI** and **Figure 15SI**). The matrix peak was not modified by the hyperfine contrast selectivity, instead it is represented by a simple Gaussian line of 0.25 MHz line width.[8b] For each field position these proton spectra were then summed up, without any further re-weighting. This procedure enabled a qualitatively correct reproduction of the Davies-ENDOR peak intensities and good agreement of their positions.

Simulated spectra of the largest and exchangeable proton hyperfine splitting of proton 1 are shown in **Figure 12SI** together with the experimental difference spectra of **1-Co**-O_2 before and after D_2O exchange in CH_2Cl_2. In **Figure 13SI,** the difference spectra of **1-Co**-O_2 in CH_2Cl_2 and CD_2Cl_2 are shown together with the simulation of the hyperfine interaction of the solvent protons 2, 3 and 4 and the matrix peak. Simulated spectra for each contributing proton and their sum spectra are shown in **Figure 14SI** (80 ns preparation pulse length) and **Figure 15SI** (160 ns preparation pulse length) together with the corresponding experimental spectra of **1-Co**-O_2 in CH_2Cl_2.

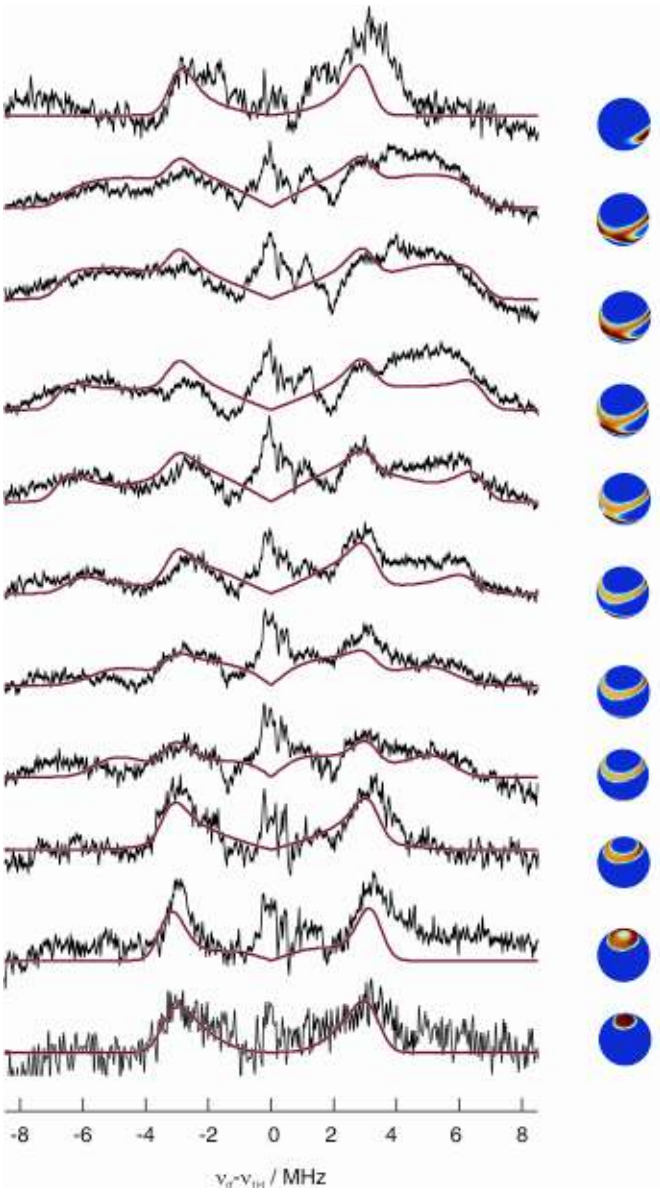

Figure 12SI: Difference Davies-ENDOR spectra of **1-Co**-O_2 before and after D_2O exchange in CH_2Cl_2 with preparation pulse length = 80 ns (black) together with the simulation (red). The orientations contributing to the experimental spectra are projected on the unit spheres.

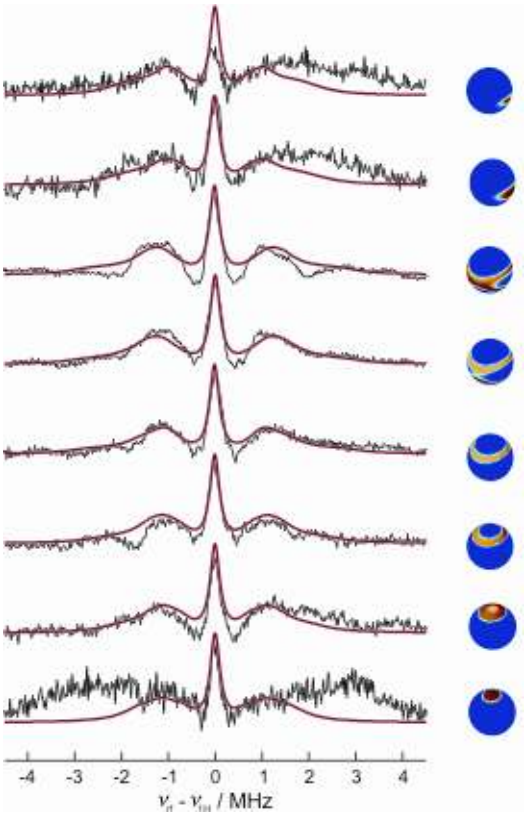

Figure 13SI: Difference Davies-ENDOR spectra of **1-Co-**O_2 in CH_2Cl_2 and in CD_2Cl_2 with preparation pulse length = 160 ns (black) together with the summed up simulated spectra of the solvent peaks (protons 2, 3 and 4) and the matrix peak (red). The orientations used in the simulations are illustrated on the unit spheres.

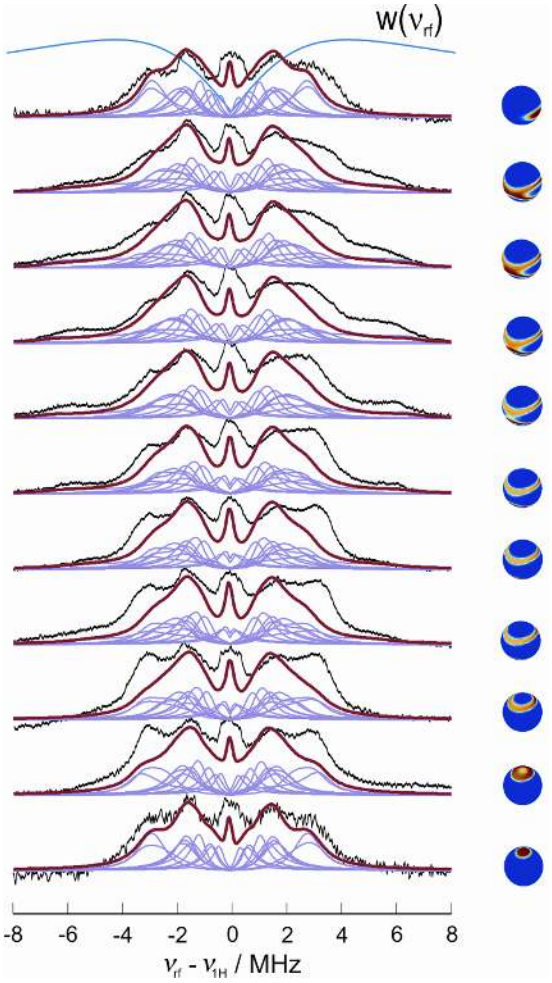

Figure 14SI: Experimental Davies-ENDOR spectra of **1-Co**-O_2 in CH_2Cl_2 with preparation pulse length = 80 ns (black) together with the sum simulation (red) and contributing individual proton spectra (blue). The weighting function $w(\nu_{rf})$ for a 80 ns preparation pulse is shown in the top spectra (blue line on top). The unit spheres depict the orientations used in the simulations.

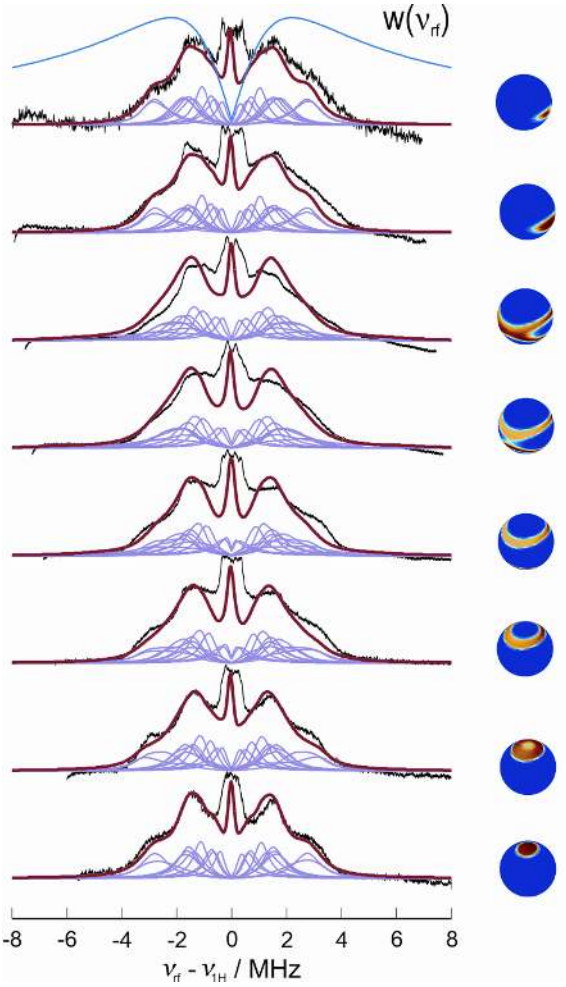

Figure 15SI: Davies-ENDOR spectra of **1-Co**-O_2 in CH_2Cl_2 with preparation pulse length = 160 ns (black) together with the sum simulation (red) and contributing individual proton spectra (blue). The weighting function $w(\nu_{rf})$ for a 160 ns preparation pulse is shown in the top spectra (blue line on top). The unit spheres depict the orientations used in the simulations.

Co-Mb-O_2 Studies

Deoxy-Co-Mb was prepared according to literature procedures in 0.01 M phosphate H_2O buffer (pH 6.0).[11] The exchange of the phosphate H_2O buffer against the phosphate D_2O buffer was achieved *via* ultrafiltration.

The CW EPR spectrum (**Figure 16SI**) agrees well with the Co-Mb CW EPR spectra reported in the literature.[12a, 12c] After D_2O buffer exchange and concentration, formation of the dioxygen adduct of deuterated Co-Mb was already complete. Therefore, no CW EPR spectrum of the deuterated Co-Mb is shown in **Figure 16SI.**

The dioxygen adduct of reconstituted Co-Mb was prepared by repetitively bubbling O_2 through a solution of reconstituted Co-Mb in potassium phosphate buffer (pH 6.0) at 20 °C. After 10 to 15 min, formation of Co-Mb-O_2 was complete. The CW EPR spectrum of Co-Mb-O_2 (**Figure 17SI**) again agrees very well with the spectra for Co-Mb-O_2 reported in the literature.[12]

X-Band CW Spectra of Co-Mb and Co-Mb-O_2

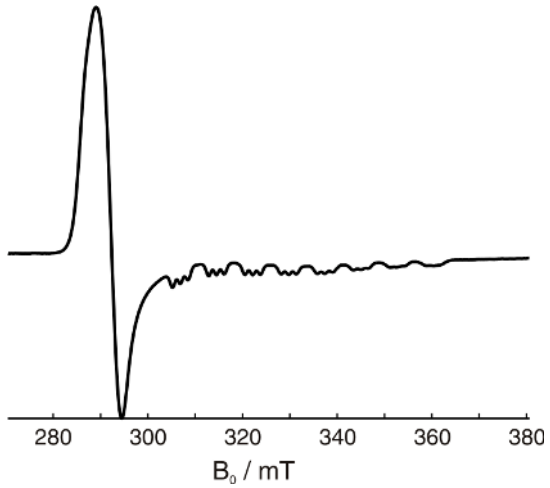

Figure 16SI: Frozen-solution X-band CW EPR spectrum of Co-Mb in H_2O phosphate buffer solution at 120 K.

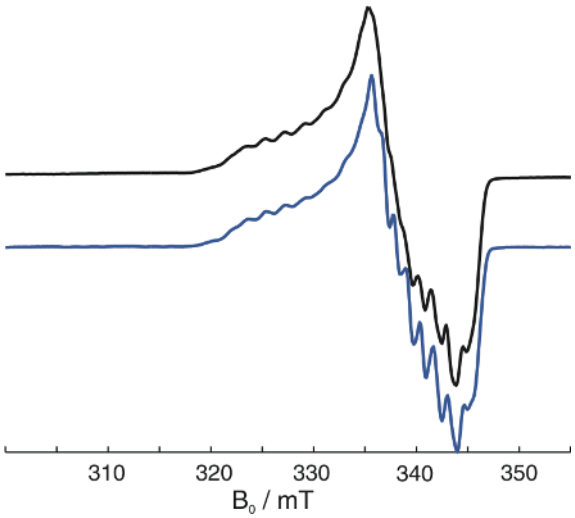

Figure 17SI: Frozen-solution X-band CW EPR spectrum of Co-Mb-O_2 at 120 K in H_2O phosphate buffer solution (black) and in D_2O phosphate buffer solution (blue).

Separation of the FID-Integral-Detected EPR Spectra of the Two Species in Co-Mb-O_2

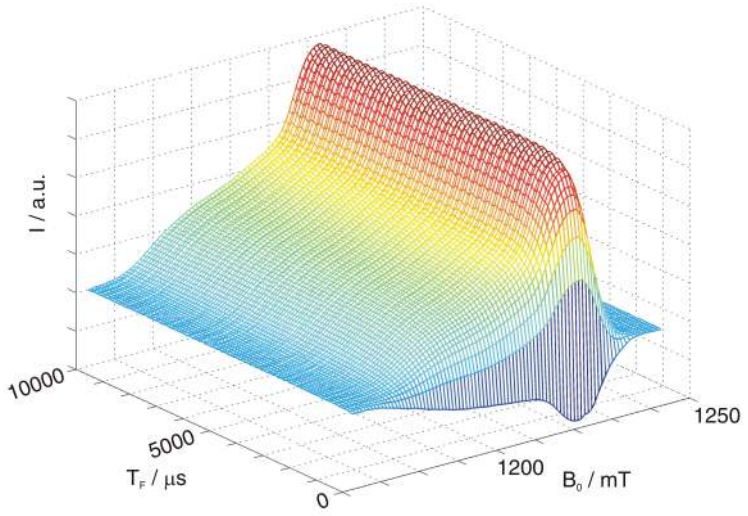

Figure 18SI: Experimental frozen-solution Q-band FID-integral-detected EPR spectra of Co-Mb-O_2 recorded with different filter times T_F (REFINE: a strong inversion pulse with flip angle 3 π followed by a free evolution time T_{F0} = 0.5 µs, ΔT_F = 100 µs followed by a selective 500 ns detection π/2 pulse was used. The decaying FID was found to be less distorted than the FID obtained by the π- π/2-detection subsequence).[13] Biexponential fits at different consecutive field positions (along the T_F dimension) were used in order to separate signal contributions from the two species.

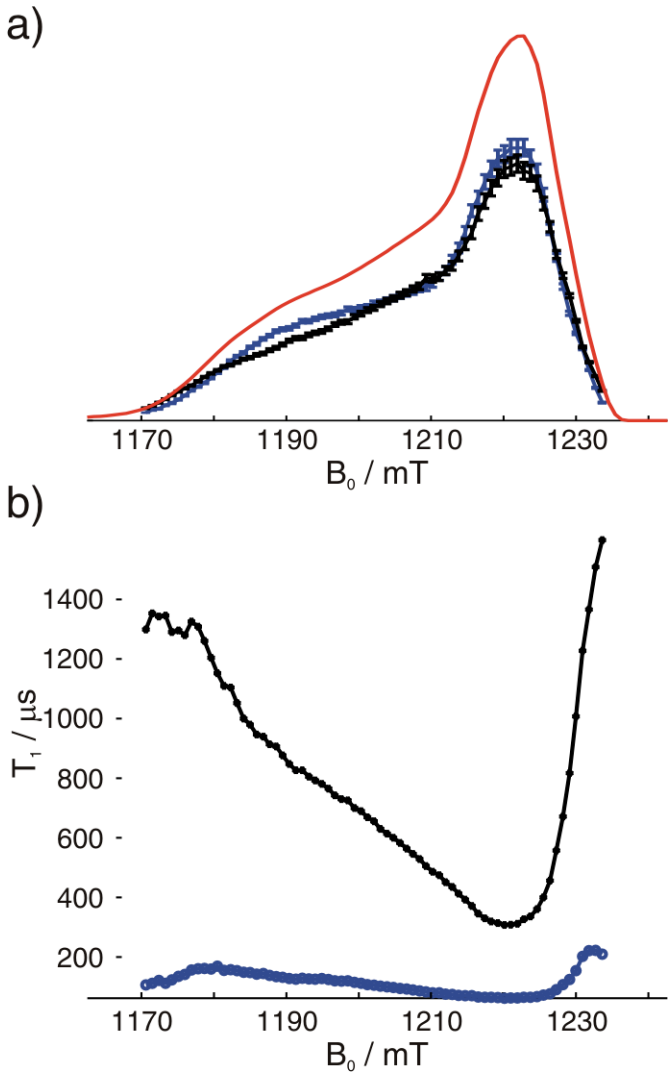

Figure 19SI: a) Experimental frozen-solution Q-band FID-integral-detected EPR spectrum of Co-Mb-O_2 (red), FID-integral-detected EPR spectrum of species 1 (blue) derived from the biexponential fits, and FID-integral-detected EPR spectrum of species 2 (black) derived from the biexponential fits. The error given is calculated from the error vectors between the experimental data and the biexponential fits. An additional error due to frequency variations was not included. b) Longitudinal relaxation

times T_1 for each Q-band field position of species 1 (blue) and species 2 (black).

Q-Band Davies-ENDOR Spectra of Co-Mb-O_2

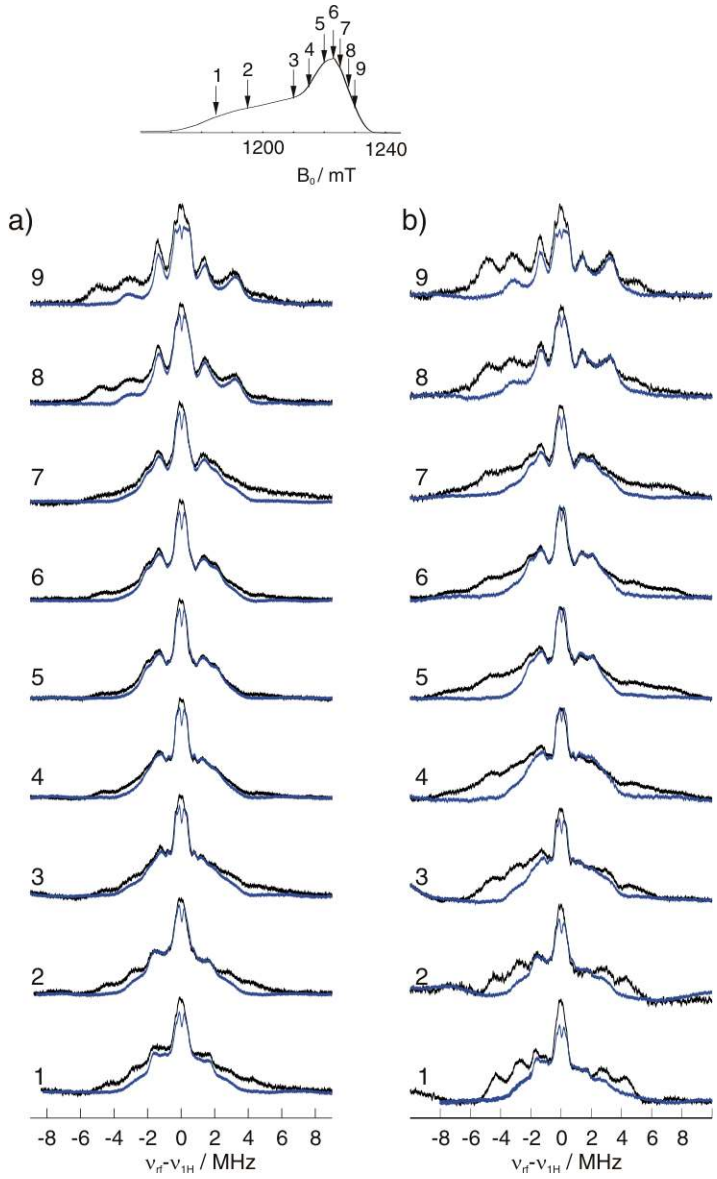

Figure 20SI: Frozen-solution Davies-ENDOR spectra of Co-Mb-O_2 in H_2O buffer solution (black), and in D_2O buffer solution (blue). Observer positions are indicated on the FID-integral-detected EPR spectra in the insets. a) Preparation pulse length = 160 ns. b) Preparation pulse length = 80 ns.

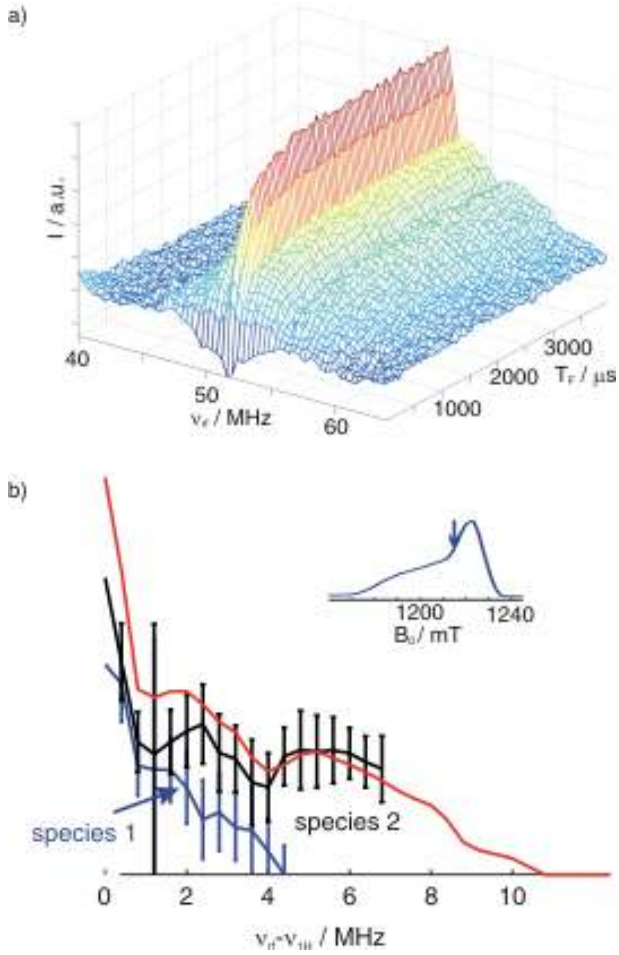

Figure 21SI: a) Experimental frozen-solution Q-band Davies-ENDOR spectra of Co-Mb-O_2 in H_2O buffer solution at the observer position 1215 mT at 13 K recorded with different filter times T_F (REFINE: a strong inversion pulse followed by a free evolution time T_{F0} = 1 µs, ΔT_F = 50 µs in advance to the Davies-ENDOR sequence was used). Each rf frequency was fitted with a biexponential decay function (along the T_F dimension) in order to separate the two overlapping species. b) High rf frequency part of the experimental Davies-ENDOR spectrum of Co-Mb-O_2 (red). The

Davies-ENDOR spectra recorded were asymmetric, having very low intensities on the low rf frequency part of the spectra. This is a known problem in Davies-ENDOR spectroscopy.

The signal contributions from the two species to the full amplitude of the spectrum were determined from the biexponential fits to the Davies-ENDOR spectra measured with different filter times T_F. The fitting was repeated at different spectral positions. In advance to the biexponential fit, a baseline correction 0^{th} order was performed with the data points at the high rf frequency range. The observer position indicated on the FID-integral-detected EPR spectrum (shown in the inset) was chosen, because here the amplitudes of species 1 and species 2 have the same magnitude, which reduces errors due to the baseline correction step of the data processing. The largest and exchangeable proton hyperfine splitting could be fitted by a monoexponential fit, providing a relaxation time of ~450 μs. This relaxation time unambiguously corresponds only to species 2.

X-Band 6-Pulse HYSCORE Spectrum of Co-Mb-O_2

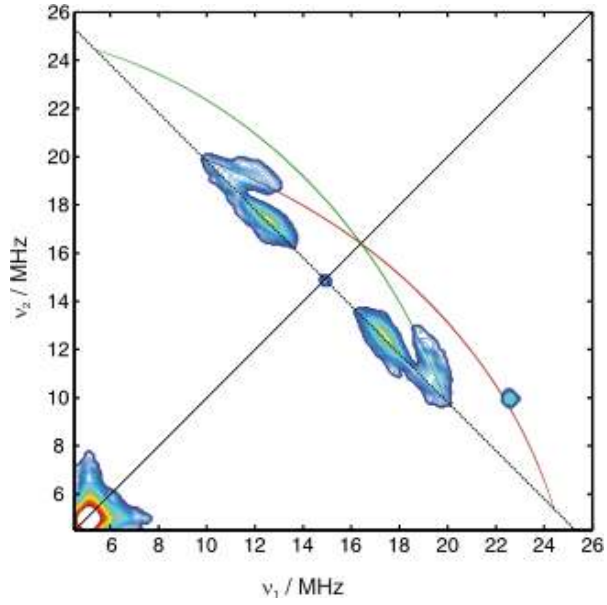

Figure 22SI: X-band 6-Pulse HYSCORE spectrum of Co-Mb-O_2 in H_2O buffer solution at 20 K and g = 2.029. The off anti-diagonal ridges stemming from the largest and exchangeable proton hyperfine splitting can clearly be distinguished from the residual anti-diagonal proton splittings. The simulated ridges (green and brown line) show the real signal extension (approximate g-values[14] and approximate hyperfine splittings of A^H = [–10 –10 19] MHz were used for the simulation). The peak at (23 MHz, 10 MHz) is a spectrometer artifact.

References

[1] J. J. P. Steward, Fujitsu Limited **2001**, MOPAC 2002.

[2] J. Vojtechovsky, K. Chu, J. Berendzen, R. M. Sweet, I. Schlichting, *Biophys. J.* **1999**, *77*, 2153-2164.

[3] S. E. V. Phillips, B. P. Schoenborn, *Nature* **1981**, *292*, 81-82.

[4] P. Weyermann, F. Diederich, *Helv. Chim. Acta* **2002**, *85*, 599-617.

[5] a) S. Stoll, C. Calle, G. Mitrikas, A. Schweiger, *J. Magn. Reson.* **2005**, *177*, 93-101. b) C. J. Calle y Richter. *ETH Diss.* No. 16883 (2006).

[6] B. Kasumaj, S. Stoll, *J. Magn. Reson.* accepted for publication.

[7] a) S. Stoll, A. Schweiger, *J. Magn. Reson.* **2006**, *178*, 42-55. b) S. Van Doorslaer, A. Schweiger, B. Kraeutler, *J. Phys. Chem. B* **2001**, *105*, 7554-7563; c) S. Van Doorslaer, R. Bachmann, A. Schweiger, *J. Phys. Chem. A* **1999**, *103*, 5446-5455.

[8] a) M. Bennati, C. T. Farrar, J. A. Bryant, S. J. Inati, V. Weis, G. J. Gerfen, P. Riggs-Gelasco, J. Stubbe, R. G. Griffin, *J. Magn. Reson.* **1999**, *138*, 232-

243; b) A. V. Astashkin, A. Kawamori, *J. Magn. Reson.* **1998**, *135*, 406-417; c) C. Fan, P. E. Doan, C. E. Davoust, B. M. Hoffman, *J. Magn. Reson.* **1992**, *98*, 62-72; d) G. C. Hurst, T. A. Henderson, R. W. Kreilick, *J. Am. Chem. Soc.* **1985**, *107*, 7294-7299; e) B. M. Hoffman, R. A. Venters, J. Martinsen, *J. Magn. Reson.* **1985**, *62*, 537-542; f) R. P. J. Merks, R. De Beer, D. Van Ormondt, *Chem. Phys. Lett.* **1979**, *61*, 142-144; g) A. E. Stillman, R. N. Schwartz, *Mol. Phys.* **1978**, *35*, 301-313.

[9] M. Baumgarten, C. J. Winscom, W. Lubitz, *Appl. Magn. Reson.* **2001**, *20*, 35-70.

[10] D. Goldfarb, B. Epel, H. Zimmermann, G. Jeschke, *J. Magn. Reson.* **2004**, *168*,75-87.

[11] F. Ascoli, M. Rosaria, R. Fanelli, E. Antonini, *Methods of Enzymology*, Academic Press, London, **1981**, *76*, pp. 72-87.

[12] a) J. Huettermann, R. Stabler in *Electron Magnetic Resonance of Disordered Systems* (Ed.: N. D. Yordanov), World Scientific, Singapore, **1989**, pp. 127-148; b) F. A. Walker, J. Bowen, *J. Am. Chem. Soc.* **1985**, *107*, 7632-7635; c) B. M. Hoffman, D. H. Petering, *Proc. Natl. Acad. Sci. USA* **1970**, *67*, 637-643.

[13] T. Maly, T. F. Prisner, *J. Magn. Reson.* **2004**, *170*, 88-96.

[14] J. C. W. Chien, L. C. Dickinson, *Proc. Natl. Acad. Sci. USA* **1972**, *69*, 2783-2787.